Nanotoxicology, June 2012; 6(4): 371–380

Can the soil bacterium *Cupriavidus necator* sense ZnO nanomaterials and aqueous Zn^{2+} differentially?

ANDREW L. NEAL[1], NADINE KABENGI[2], ARTHUR GRIDER[3], & PAUL M. BERTSCH[2]

[1]*Sustainable Soils and Grassland Systems Department, Rothamsted Research, West Common, Hertfordshire, UK,* [2]*Department of Plant and Soil Sciences, University of Kentucky, Lexington, Kentucky, and* [3]*Department of Foods and Nutrition, The University of Georgia, Athens, Georgia, USA*

(Received 10 January 2011; accepted 24 March 2011)

Abstract

Synthetic metal oxide nanomaterials exert toxicity *via* two general mechanisms: Release of free ions at concentrations which exert toxic effects upon the target cell, or specific surface-mediated physicochemical processes leading to the formation of hydroxyl free radicals and other reactive oxygen species which act to disrupt cell membranes and organelles. From a regulatory standpoint this presents a potential problem since it is not trivial to detect free metal ions in the presence of nanoparticles in biological or natural media. This makes efforts to identify the route of uptake difficult. Although *in vitro* studies of zinc oxide nanoparticles suggest that toxicity to the soil bacterium *Cupriavidus necator* is exerted in a similar manner to zinc acetate, we found no free Zn ion is associated with nanoparticle suspensions. The proteome of cells subjected to equal concentrations of either the nanoparticle or zinc acetate suggest that the mode of toxicity is quite different for the two forms of Zn, with a number of membrane-associated proteins up-expressed in response to nanoparticle exposure. Our data suggests that nanoparticles act to interrupt cell membranes thereby causing cell death rather than exerting a strictly toxic effect. We also identify potentially useful genes to serve as biomarkers of membrane disruption in toxicogenomic studies with nanoparticles or to engineer biosensor organisms.

Keywords: *Microbiology, proteomics, toxicology, environmental toxicology, nanoparticles*

Introduction

A key question raised by the rapid adoption of nanotechnology across a wide variety of technologies from electronics to personal care products is release to the environment and exposure of ecoreceptors to traditional metal contaminants present in a new form. This exposure presents a potential cause for concern in respect to how regulatory bodies treat eventual disposal, either inadvertent or intended, to the environment. The salient question is whether such new forms of metals (as nanoparticles) should be treated effectively as aqueous ions, falling under a legal framework established upon a wealth of information regarding biological and environmental effects of metal exposure, or whether nanomaterials should be treated as novel forms of environmental contaminants. Implicit in the adoption of the latter is acceptance that environmental exposure to nanomaterials occurs outside any evidence-based framework until relative toxicity of new products is compared to the equivalent free metal ion. It is therefore important to develop data establishing the relative toxicity of nanomaterials and to determine whether any observed toxicity occurs through the relatively well established mechanisms ascribed to aqueous ions or whether new paradigms of toxicity have to be elucidated.

A number of studies have demonstrated that, for metal and metal oxide nanomaterials it is, for example, dissolved silver (Ag), zinc (Zn), copper (Cu) or cadmium (Cd) released from nanoparticles that are responsible for the observed toxicity (Derfus et al. 2004; Brunner et al. 2006; Franklin et al. 2007; Karlsson et al. 2008; Aruoja et al. 2009; Studer et al. 2010). In this instance, regulation of disposal or environmental exposure may reasonably be based upon toxicological studies of aqueous ions. However, the wide variety of synthesis pathways for the same nanoparticle – ranging from laser vapor/condensation (Samy El-Shall et al. 1995) to refluxing over-saturated

Correspondence: Dr Andrew L. Neal, PhD, Sustainable Soils and Grassland Systems Department, Rothamsted Research, West Common, Hertfordshire, AL5 2JQ, UK. Tel: +44 1582 763133. E-mail: andy.neal@bbsrc.ac.uk

ISSN 1743-5390 print/ISSN 1743-5404 online © 2012 Informa UK, Ltd.
DOI: 10.3109/17435390.2011.579633

solutions of zinc acetylacetonate hydrate in 1-butanol and isobutanol (Ambrožič et al. 2010) for ZnO alone – means that it is not always clear whether free aqueous ions are present in nanoparticle suspensions. In such situations it is important to identify the main toxicological mechanism, a problem confounded by the fact that descriptions of synthesis rarely consider the presence of aqueous ions, concentrating instead on the properties of the particles themselves. Equilibrium dialysis (1 kDa molecular weight cut-off, pore size approximately 1 nm) can be used to identify free aqueous ions derived from nanoparticles in simple solutions (Franklin et al. 2007) however, in complex media or in the presence of organisms where free metal ions may associate with membranes etc. it is often difficult to differentiate between effects of nanoparticulate species and the associated ionic species (Brunner et al. 2006) making assessment of specific nanoparticle risks imprecise. Additionally, many spectroscopic techniques may fail to identify relatively low concentrations of free ions associated with nanoparticle suspensions.

In the face of these obstacles to unequivocally identifying the mechanisms of toxicity of nanoparticles, we have chosen to study the cellular (proteome) response of a common soil bacterium to ZnO nanoparticles and compared the response to that observed towards a zinc acetate solution. *Cupriavidus necator*, originally isolated from soil (Don and Pemberton 1981), is an ideal model for the important group of plant-associated microorganisms, the rhizobacteria. In common with other well studied rhizobacteria, *C. necator* exhibits high catabolic diversity (the genome and associated plasmids contains determinants for 11 of the 12 main aromatic compound degradation pathways, Pérez-Pantoja et al. 2008). In addition to mineralization of plant-derived and anthropogenic aromatic compounds, *C. necator* also influences the soil carbon cycle by producing polyhydroxyalkanoate carbon and energy storage compounds common to prokaryotes. We demonstrate that although ZnO nanoparticles and zinc acetate appear similarly toxic to *C. necator*, the cellular response to ZnO nanoparticles indicates an absence of Zn ions from nanoparticle suspensions. In fact the cellular response to the two forms of Zn is quite different with an emphasis on up-expression of membrane proteins in response to nanoparticle exposure.

Materials and methods

Characterization of ZnO nanomaterials

Pinnacle[AF] ZnO nanoparticle (ZnO-NP) suspension was purchased from Applied Nanoworks (now Auterra Inc., Malta, NY; www.auterrainc.com). The product was reported by the manufacturers to have a primary particle size of 2–6 nm and a surface area of 250 $m^2 g^{-1}$. Acetate (OAc) was also reported to be present in the suspension. Subsamples were characterized along with stock and aqueous dilutions of the suspension as described below where appropriate. Total zinc concentration was determined with inductively coupled plasma mass spectrometry (ICP-MS; Elan DRC Plus, Perkin Elmer-Sciex, Waltham, MA, USA). Total OAc concentration of the received suspension and experimental suspensions were determined using ion chromatography (DX-500, Dionex, Sunnyvale, CA, USA). Particle images were obtained using a Philips/FEI Technai 20 transmission electron microscope (TEM) operating at 200 keV. The TEM micrographs revealed particle morphology and size. Samples were prepared by placing a drop of diluted sample on a holey carbon-coated copper grid and allowing the solvent to evaporate in air. In a similar fashion, the XRD pattern recorded for ZnO-NPs shares more charateristics with Zn-OAc than ZnO (Figure 3).

ZnO-NPs were characterized and compared to zinc oxide mineral (ZnO-wurtzite) and zinc acetate (Zn-OAc) standards by FT-Raman spectroscopy. Spectra were collected on a Nicolet™ FT-Raman 960-*ESP* spectrometer, equipped with a Ge liquid-N_2 cooled detector and 1064 nm excitation from a 2 W Nd:YVO_4 laser. Samples were characterized as powders.

Bacterial culture and exposure to nanomaterials

The Beta-proteobacterium *Cupriavidus necator* JMP134 (also known as *Ralstonia eutropha*, *Wautersia eutropha*, *Alcaligenes eutropha* and *C. pinatubonensis*) was acquired from the American Type Culture Collection (strain 17699). Cells were grown from frozen stocks on Nutrient Agar (Fisher Scientific, Hampton, NH, USA) for each experiment. Biomass was produced by culture in Nutrient Broth at 25°C with agitation (150 rpm). Overnight cultures were harvested by centrifugation and washed three times in 5 mM Piperazine-1,4-bis(2-ethanesulfonic acid) buffer (PIPES, Sigma P6757), pH 7.2. Washed cells were then transferred to a medium containing 10 mM PIPES, 5 mM $Na(O_2CCH_3)_2$ (Na-OAc) and cultured under the same conditions for 8 h. Cells were then diluted to an optical density at 410 nm (OD_{410}) of 0.06 for use in growth experiments.

Growth and OAc utilization experiments were conducted in a 96-well plate format, allowing treatment replication and a number of treatments to be conducted simultaneously. Varying amounts of either

ZnO-NPs or Zn-OAc were added to provide a range of Zn concentrations from 25 nM–100 μM. At each time point, three replicates for each treatment were sampled by collecting the entire contents (200 μL) of pre-determined wells. The effect of the Zn-form and various concentrations upon cell growth was followed by monitoring OD_{410}. Growth rate (μ) was estimated from the linear portion of the growth curve, expressed according to $\mu = (\ln OD_{t=0}/\ln OD_{t=n})/t$: where OD represents OD_{410} and t represents time. Mean μ for each treatment were compared using an analysis of variance, employing time as a covariate. Significant differences between μ in the absence of any added Zn and each treatment were determined using Bonferroni comparisons ($\alpha = 0.05$). OAc-utilization was determined by collecting culture samples (1 mL), filtering (<0.2 μm) to remove cells, and measuring OAc concentration by ion chromatography. Total metal exposures at which OAc-utilization was measured were limited to 50, 25, 1 and 0.1 μM total Zn, based upon consideration of growth rates. Data for OAc-utilization was analyzed the same way as growth rate data.

Two-dimensional gel electrophoresis

Soluble proteins were extracted from bacterial pellets using 1 mL of extraction buffer containing 40 mM TRIS (tris(hydroxymethyl)aminomethane) base, protease inhibitor cocktail (1.04 μM AEBSF, 0.8 nM aprotinin, 20 nM leupeptin, 40 nM bestatin, 0.15 μM pepstatin A, 0.14 μM E-64), 150 U benzonase. The cells were lysed in this buffer by sonication and the lysate centrifuged at 13,000 *g* for 20 min at 4°C. The supernatant was removed and saved as the soluble protein fraction at −80°C. The resulting pellet was resuspended in the extraction buffer and the solution centrifuged again. The proteins within the pellet were extracted in 0.3 mL of insoluble protein extraction buffer containing 5 mmol L^{-1} urea, 2 mmol L^{-1} thiourea, 2% (w/v) CHAPS (3-[(3-cholamidopropyl) dimethylammonio]-1-proanesulfonate), 2% (w/v) SB 3–10 (*N*-decyl-*N*,*N*-dimethyl-3-ammonio-1-propanesulfonate), 40 mmol L^{-1} TRIS base, 0.2% carrier ampholytes pH 3–10, 2 mmol L^{-1} tributyl phosphine. The samples were sonicated twice for 10 sec and then vortexed for 4 min. The samples were incubated overnight at −80°C, then thawed and vortexed for 5 min. The samples were centrifuged at 13,000 *g* for 10 min at room temperature. The supernatant containing the extracted pellet proteins was transferred to fresh microfuge tubes. The amount of protein in the soluble protein samples was determined by the RC/DC Protein Assay (Bio-Rad), based upon the Lowry procedure (Lowry et al. 1951). The protein concentration of the insoluble protein samples was determined using the Bradford Protein Assay (Bradford 1976; Zor and Selinger 1996).

The volume of sample containing either 300 μg soluble or 200 μg insoluble proteins was reduced and alkylated prior to 2-D GE. The protein solution was reduced by adding 25 μL of 200 mmol L^{-1} TBP per mL and incubating at room temperature for 1 h. The protein solution was then alkylated by adding 30 μL of 500 mmol L^{-1} iodoacetamide and incubating for 1.5 h at room temperature. Protein was precipitated with acetone and dissolved in rehydration buffer prior to isoelectric focusing.

2-D gel electrophoresis. A total of 300 μg of soluble protein, or 200 μg of insoluble protein, was loaded on to pH 3–10 immobilized pH gradient isoelectric focusing strips (Bio-Rad). The strips were actively rehydrated overnight in insoluble protein buffer containing 0.002% Bromophenol blue. Focusing was performed at 20°C for 20 kV-hours. Focused strips were equilibrated for 20 min with SDS-PAGE sample buffer containing 6 mol L^{-1} urea, 375 mmol L^{-1} TRIS-HCl, pH 8.8, 2% (w/v) SDS, 20% (v/v) glycerol, 2 mmol L^{-1} TBP and 0.00125% (w/v) Bromophenol blue. Strips containing focused soluble proteins were placed on top of denaturing 12.5% acrylamide gels with 3% stacking gels while those containing focused insoluble proteins were placed on top of denaturing 10% acrylamide gels with 3% stacking gels. The second dimension separating gels were run using 30 mA gel^{-1} constant current. The gels were fixed in 40% methanol:10% acetic acid for at least 1 h, then rinsed with ultrapure water three times for 10 min each time, and stained overnight with colloidal blue silver (Candiano et al. 2004). Stained gels were de-stained in ultrapure water until the background was minimal. The gel images were digitized using a flatbed scanner and analyzed using the Phoretix 2D densitometry program. Spot densities exhibiting two-fold or greater differences were excised and analyzed by mass spectrometry at the Proteomics and Mass Spectrometry Core Facility of The Medical College of Georgia, Augusta GA, USA.

Results

Characterization of zinc oxide nanoparticles

The total zinc concentration of the ZnO-NP stock solution was determined to be 71.8 g L^{-1} (standard deviation [SD], 3.1 g L^{-1}), and the acetate concentration 3.01 M (SD, 0.14 μM). Drying ZnO-NPs at

room temperature resulted in the evaporation of 55.5% of the acetate initially present (SD 1.14%). In conjunction with data collected from FT-Raman spectroscopy (see below), this appeared to correspond to a free acetate population present in the ZnO-NP stock solution. TE micrographs show the primary ZnO-NPs to be between 1 and 3 nm in diameter (Figure 1).

FT-Raman spectroscopy of zinc oxide (ZnO, wurtzite structure, C^4_{6v} space group) and zinc acetate (Zn-OAc) standard compounds are shown in Figure 2 and compare well with published spectra (Yang et al. 2005; Ben Yahia et al. 2008; Kim et al. 2010). For ZnO, the principal peaks with Raman shifts of 438 and 99 cm^{-1} are due to the E_2^{high} and E_2^{low} phonon modes respectively. Other peaks are due to the (E_2^{high} - E_2^{low}) mode at 333 cm^{-1} and the A_1 transverse optical mode at 381 cm^{-1}. A broad second order mode is observed at approximately 1105 cm^{-1}. For Zn-OAc, contributions to the spectra arise from the Zn centre, the B_{2g} and A_{1g} modes at 227 and 264 cm^{-1}, respectively, due to ZnO_4 vibrations, Zn-OH_2 symmetric stretch (ν) at 413 cm^{-1}, and due to the acetate ligand at 954 cm^{-1} (A_1 mode, νC-C), 696 cm^{-1} (A_1 mode, OCO bend), 476 cm^{-1} (B_1 mode, OCO rocking), 1362 cm^{-1} (CH_3 bend) and 1467 cm^{-1} (νC-O). With the exception of some structural differences below 200 cm^{-1}, the FT-Raman spectrum collected from the ZnO-NPs is very similar to that collected from Zn-OAc. All the major vibrational modes of Zn-OAc are observed, none of the ZnO modes are clearly resolvable. Reduction in the intensity of the E_2^{high} ZnO mode has previously been observed for acetate-stabilized ZnO-NPs (Yang et al. 2005) and it is possible that this intensity reduction, combined with the strong vibrations due to OAc groups, account for the lack of obvious ZnO vibrational modes associated with ZnO-NPs. Additionally, a characteristic red-shift of the νC-O vibration has also been observed for acetate-stabilized ZnO-NPs (Yang et al. 2005). The shift has been presented as evidence for a lack of free-OAc groups associated with the ZnO-NPs, which are instead bonded to the ZnO surface (Yang et al. 2005). For our samples, νC-O is shifted from 1467 cm^{-1} for Zn-OAc to 1452 cm^{-1} for ZnO-NPs, a red shift of 15 cm^{-1}.

C. necator growth rate and acetate utilization

To determine whether exposure to the two forms of Zn affected *C. necator* growth and acetate catabolism rates, cells were exposed to increasing concentrations of zinc either as Zn(II) (Zn-OAc) or ZnO-NPs in batch culture. A significant, dose-dependent effect of both forms of Zn upon growth rate (μ) was observed (Figure 4). No growth was evident at Zn concentrations above 50 μM for either ZnO-NPs or Zn-OAc. Statistical analysis indicated μ at 25 μM Zn was significantly reduced ($p < 0.05$) compared to the baseline μ of 0.011 h^{-1}, determined from cells grown in the absence of Zn. At 25 μM, there was no significant difference between the effects of the two forms of Zn. At total Zn concentrations below 25 μM, μ was not statistically different from the baseline down to a concentration of 25 nM: Again no differences between the two Zn forms were detected. However, the growth response across the 1000–25 nM Zn range does differ between the two forms: With the exception of 100 nM, μ at all other concentrations of ZnO-NPs was identical to the baseline growth in contrast to Zn-OAc, where μ shows an optimum utilization rate at 100 nM of 0.013 h^{-1} with reduced growth rates both at higher and lower Zn concentrations. This can be interpreted as a response of cell growth rate to the availability of Zn(II), an essential element for growth

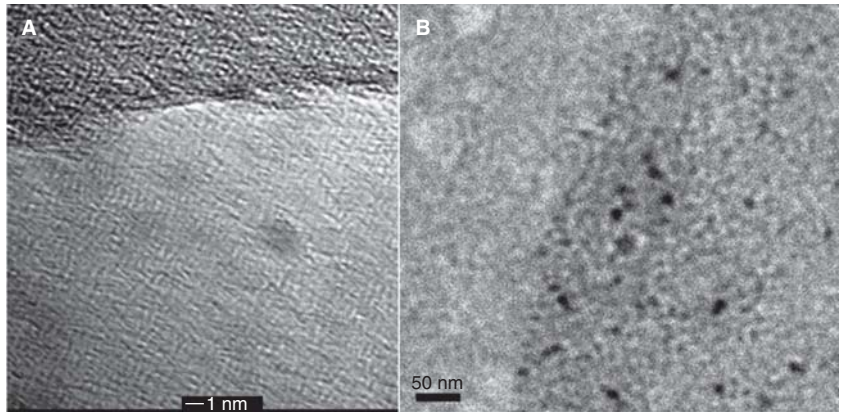

Figure 1. Zinc oxide nanoparticles observed by transmission electron microscopy after allowing a dilute nanoparticle suspension to dry on the surface of a holey carbon coated copper support.

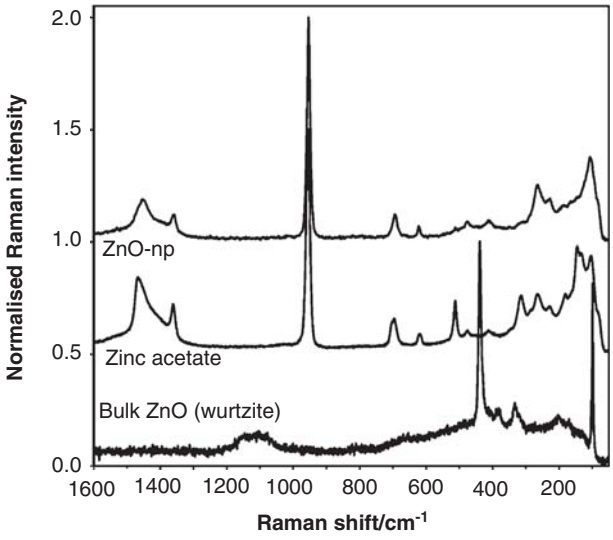

Figure 2. Powder Fourier-transform Raman spectra of the standard materials zinc acetate and the zinc oxide mineral wurtzite compared to the spectrum collected from dried zinc oxide nanoparticles. There is little evidence of the principal wurtzite modes in the nanoparticle spectrum. The C-O stretching mode of zinc acetate at 1467 cm^{-1} is red shifted in the ZnO nanoparticle spectrum suggestive of acetate groups coordinated to the ZnO surface.

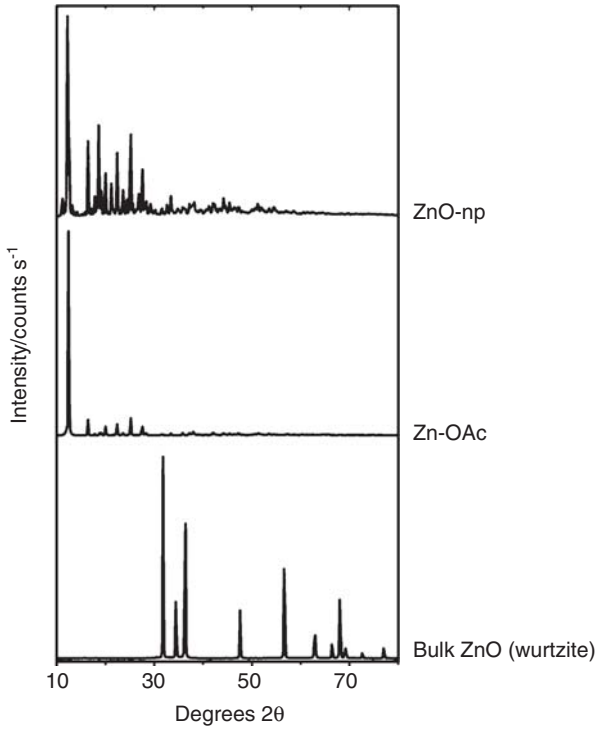

Figure 3. Cu Kα X-ray diffraction patterns recorded for powders of the standard materials zinc acetate and the zinc oxide mineral wurtzite compared to the spectrum collected from dried zinc oxide nanoparticles.

but which is also toxic at elevated concentrations. Following this line of argument, the response of growth rate to ZnO-NP concentrations would suggest that far less bio-available Zn(II) was present in suspensions of the ZnO nanoparticles compared to the Zn-OAc solutions.

Based upon analysis of growth rates, the effect of Zn upon the utilization of acetate by *C. necator* cultures was limited to 50, 25, 1.0 and 0.1 μM. In the absence of Zn, culture acetate ulitization rates were measured at 4.2 nM-OAc h^{-1} (standard error, 0.5 nM-OAc h^{-1}). At Zn concentrations of 50 and 25 μM, OAc utilization rates for both forms of Zn were significantly ($p < 0.05$) reduced to approximately 3 nM-OAc h^{-1} (Figure 5). It is notable that in both cases, significant OAc utilization was observed at 50 μM total Zn in the absence of any measureable growth (Figure 4). This suggests that Zn exerts such high metabolic costs to overcome toxicity effects that growth ceases. At 1.0 and 0.1 μM ZnO-NPs, OAc utilization was not significantly different from that in cultures growing in the absence of Zn. However, at both concentrations of Zn-OAc acetate, utilization rates were significantly greater than the baseline rate, again suggesting a role for bioavailable Zn(II) in increasing growth in the presence of Zn-OAc not observed with the ZnO-NP exposed bacteria. The fact that OAc utilization was higher for 0.1 μM Zn-OAc than for 1 μM suggests that some inhibitory effect is exerted by Zn at 1 μM, although the net effect of this inhibition and the greater OAc utilization in response to bioavailable Zn results in an increased OAc utilization rate compared to cells growing in the absence of Zn (baseline OAc utilization rate).

Proteome analysis by 2-D electrophoresis and tandem mass spectrometry

Separate analyses were conducted for soluble and insoluble proteins isolated from cells exposed to 0.1 and 1 mM of Zn-OAc and ZnO-NPs, as well as cells not exposed to either form of Zn (Zn-free controls). Two gels were analyzed for each concentration: treatment combination, resulting in a total of ten gels. Quantitative intensity analysis of spots identified in Figure 6 revealed significant differences in the proteome response of cells exposed to the two forms of Zn. Following intensity quantification, some protein spots were identified on gels from cells exposed to Zn with a greater than two-fold increase in intensity compared to unexposed cells and these spots were excised and identified by tandem mass spectrometry. In total, four soluble proteins and three insoluble proteins were characterized as being associated with (presenting a greater than two-fold increase) cell exposure to Zn-OAc, whilst two soluble and four insoluble proteins were characterized as being

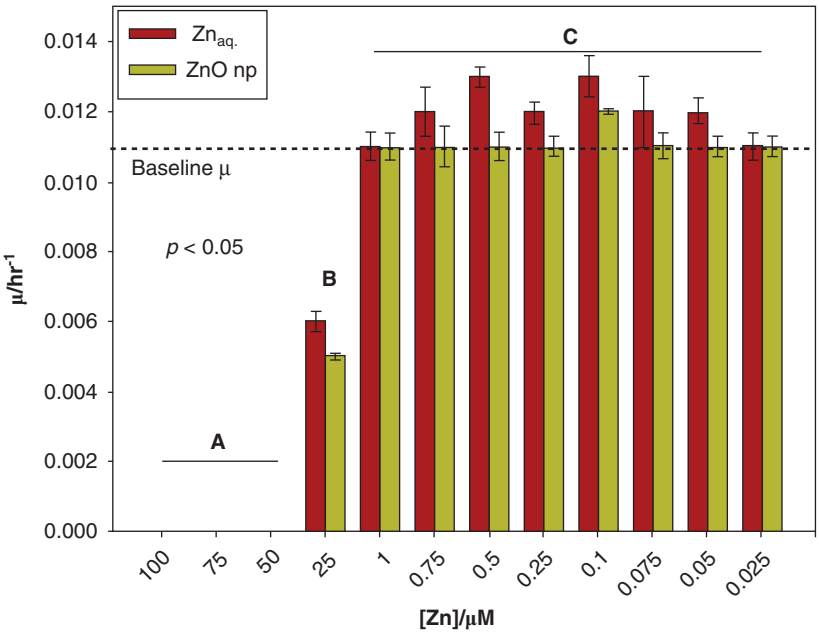

Figure 4. Relative growth rate (μ, ± standard error of the mean) of *Cupriavidus necator* in a simple PIPES-buffered medium exposed to varying concentrations of zinc (Zn) either as aqueous zinc acetate ($Zn_{aq.}$) or as zinc oxide nanoparticles (ZnO-NPs). μ was calculated from the linear part of the growth curve and multiple comparisons of the linear regressions divided the observed rates into three groups ($p < 0.05$): Group A where no growth was observed; B where relative growth rates were significantly reduced compared to baseline growth measured in the absence of any added zinc; and C where growth rates were not significantly different from baseline growth. Baseline μ of 0.011 h^{-1} is indicated by the dashed line.

associated with exposure to ZnO NPs. These proteins were consistently observed in all gels of each treatment, and are listed in Table I. Those proteins showing a two-fold or higher increase in response to Zn-OAc exposure were largely involved in cellular metabolic processes such as aconitase A (Reut_A2331, GI:72119430), NAD-dependent aldehyde dehydrogenase (Reut_B4869, GI:73538694), and phasin

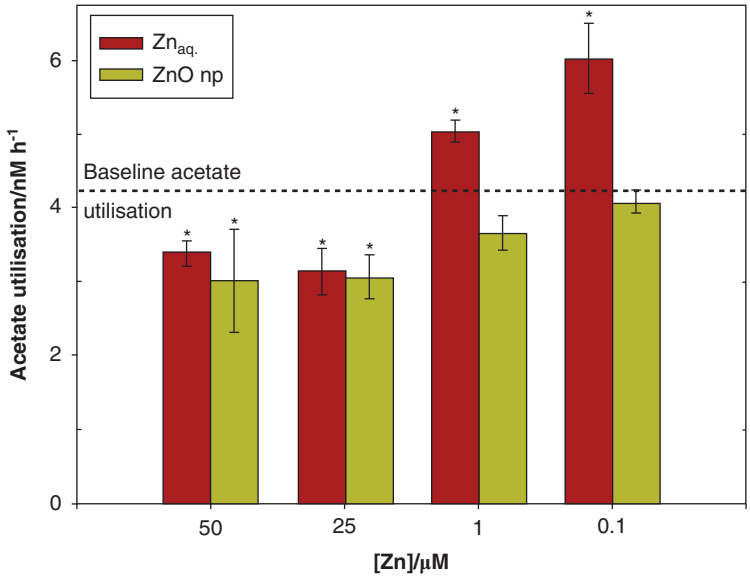

Figure 5. Rates of acetate utilisation (± standard error of the mean) determined from cultures of *Cupriavidus necator* exposed to varying concentrations of zinc (Zn) either as aqueous zinc acetate ($Zn_{aq.}$) or zinc oxide nanoparticles (ZnO-NPs). Maximum acetate utilisation rates were determined from the linear portion of the acetate utilisation curve and rates were compared statistically to the baseline rate measured in the absence of any added zinc, shown as a dashed line. Asterisks indicate a significantly different rate from the baseline rate ($p < 0.05$).

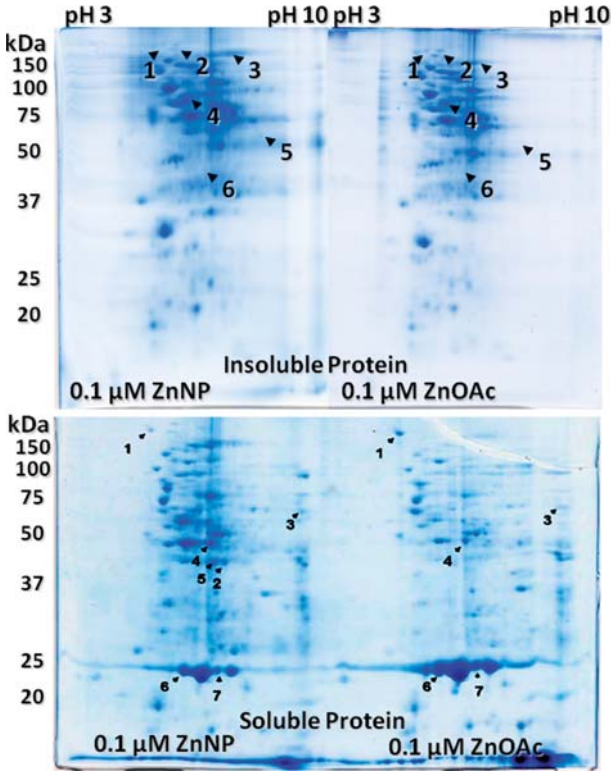

Figure 6. Representative two-dimensional electrophoresis of soluble and insoluble proteins purified from *Cupriavidus necator* exposed to 0.1 µM zinc, either as the aqueous ion from zinc acetate (ZnOAc) or ZnO nanoparticles (ZnO-NPs). Protein spots identified by numerals are described in Table I.

(Reut_B4349, GI:73537699): Other proteins were involved in controlling cellular response to stimuli (Two-component Fis family transcriptional regulator, Reut_A2947, GI:73542354). In contrast, proteins increased in the presence of ZnO nanoparticles are more characteristic of protein synthesis (GTPase-translation elongation factor Tu, Reut_A3182, GI:73542866) and secretion (Signal recognition particle, Reut_A2947, GI:73542631; LysM-containing uncharacterized protein, Reut_A3409, GI:72120504).

Discussion

A key criticism of much nanotoxicological research to date is that few studies directly compare nanomaterials with the parent free metal ion. We have directly compared ZnO NPs with the aqueous Zn(II) ion to develop a better understanding of the relative toxicity of the two phases, and also to determine whether Zn toxicity is exerted via the same or different cellular mechanisms. Our studies indicate that, due to the high concentration of acetate supplied with the ZnO-NPs, it is difficult to establish the true chemical nature of the nanomaterial. Particles are observed by TEM falling within the 1–3 nm size range (Figure 1). However, both FT-Raman spectroscopy (Figure 2) and X-ray diffraction (XRD, Figure 3) fail to distinguish between the nanomaterial and a Zn-OAc standard and emphasize the complexity of determining whether nanomaterials should be treated as new materials or as aqueous metal ions with respect to environmental exposure.

The issue of the presence of Zn(II) in nanomaterial suspensions is directly addressed by observing *C. necator* growth and catabolic activity. Zn(II) acts as an important co-factor for a number of enzymes including DNA and RNA polymerases, alkaline phosphatases, carbonic anhydrases, carboxypeptidases and alcohol dehydrogenases (Kimura 1993), and has been shown to be required for optimal growth of *C. necator* (Respaske and Respaske 1976). However, at elevated concentrations Zn(II) exerts toxic activity: Interacting with sulfhydryl groups of enzymes and other important cellular proteins and aggressively inhibiting respiratory electron transport (Kasahara and Anraku 1974; Beard et al. 1995). We conducted cell exposure assays in a simple solution of PIPES buffer and acetate, specifically lacking in essential nutrients. Therefore we expected to be able to observe any effects of Zn(II) upon cellular activity, both positive or negative. In this respect treatments including Zn-OAc can be viewed as an effective 'positive control', where both growth promotion and inhibition should be observed. If free Zn(II) ions are present in nanomaterial suspensions their effect may also be observed as growth promotion at lower ZnO-NP concentrations. The effects of *C. necator* exposure to Zn-OAc solutions (Figures 4 and 5) clearly demonstrate that at concentrations greater than 25 µM, Zn(II) significantly reduces both cellular growth rate and OAc utilization compared to cells incubated in the background PIPES/OAc solution. At Zn(II) concentrations below 1 µM, both growth rate and OAc utilization are increased, although only the latter is increased significantly. By comparison, although both growth rate and OAc utilization are also significantly reduced by a 25 µM ZnO-NP suspension, no growth or catabolic promotion is observed at lower concentrations of the nanomaterial. This is indicative of a lack of bioavailable zinc, as Zn(II), in nanomaterial suspensions and confirms the existence of particles. It also suggests that although the toxicity of Zn(II) and ZnO-NP appear similar, the mechanism(s) of growth and catabolism reduction cannot be common to the two Zn forms since there is a very low level of free Zn(II) associated with the nanomaterial.

Evidence for different mechanisms of growth and catabolic reduction between Zn(II) and ZnO-NP can be drawn by comparing the proteome response of

Table I. Identification and function of *Cupriavidus necator* JMP134 proteins showing greater than two-fold increase in expression in the presence of Zinc acetate (Zn-OAc) or ZnO nanoparticles (ZnO-NPs). Protein spots relate to those shown in Figure 6.

Treatment and Protein spot number	MS/MS identification	*Reut* gene locus[a]	Putative function[a]	Accession number	Fold Change
	Soluble proteins				
ZnO-NPs Spot 1	Phosphoribosylformylglycinamide synthase, PurL	*A1390*	Purine biosynthesis	72118497	>2
Zn-OAc Spot 2	Chromosome segregation ATPase	*A3355*	Chromosome organization	73543037	>2
Zn-OAc Spot 3	Aconitase A, AcnA	*A2331*	Metabolic processes	72119430	>2
Zn-OAc Spot 4	NAD-dependant aldehyde dehydrogenase	*B4869*	Cellular ldehyde metabolic processes	73538694	>2
ZnO-NPs Spot 5	Uncharacterized, LysM-containing domain	*A3409*	Membrane-associated protein	72120504	>2
Zn-OAc Spot 6	Not identified	-	-	-	>2
	Insoluble proteins				
Zn-OAc Spot 1	Two-component, σ^{54}-specific, Fis family transcriptional regulator	*A2669*	Signal transduction system	73542354	4
ZnO-NPs Spot 2	Aspartate/Tyrosine/Aromatic amino transferase	*A1050*	Cellular amino acid metabolic processes	73540753	2–4
ZnO-NPs Spot 3	Signal Recognition Particle, subunit SRP54	*A2947*	SRP-dependant co-translational protein, membrane targeted	73542631	2–3
ZnO-NPs Spot 4	GTPase-translation elongation factor Tu	*A3182*	Protein biosynthesis	73542866	2–4
ZnO-NPs Spot 5	Integrase	*A2191*	DNA integration	73541878	2–8
Zn-OAc Spot 6	Phasin	*B4349*	Polyhydroxyalkanoate granule-associated protein	73537699	2
Zn-OAc Spot 7	Phasin	*B4349*	Polyhydroxyalkanoate granule-associated protein	73537699	2–3

[a]www.ncbi.nlm.nih.gov/Taxonomy/Browser/wwwtax.cgi?id = 264198.

C. necator exposed to the two forms of zinc since a common mode of toxicity would be expected to elicit a common proteome response. In fact, both soluble and insoluble proteins expressed by *C. necator* are qualitatively different, dependent upon the form of Zn to which cells are exposed (see Table I). This supports the assumption of different modes of toxicity between Zn(II) and ZnO-NPs. Moreover, the specific proteins with increased expression under exposure to each Zn species also suggest a quite different cellular response to toxicity induced by aqueous Zn(II) compared to the ZnO-NPs. Under Zn(II) exposure, up-expressed proteins (*Zn(II)-up*) are generally related to metabolic processes such as Aconitase A, NAD-dependent aldehyde dehydrogenase and phasin: Aconitase is a key protein involved in acetate assimilation, converting citrate to aconitate, an intermediate in the isomerization of citrate to isocitrate in the citric acid cycle (Nakano and Fukaya 2008); phasin is involved in the formation of carbonosomes, formed when excess amounts of carbon are present while growth is limited by a lack of other essential nutrients such as nitrogen, phosphorous or oxygen etc. (Steinbüchel and Schlegel 1989; York et al. 2001; Pötter et al. 2002) as is the case in our simple PIPES/acetate experimental medium; other *Zn(II)-up* are involved with chromosome segregation (chromosome segregation ATPase), controlling the partitioning of daughter chromosomes into cells during cell division, and a two component, σ^{54}-specific, Fis family transcriptional regulator involved in signal transduction in response to environmental cues, shown to be involved in cellular responses of *Pseudomonas putida* to canola root exudates (Cheng et al. 2009) and invasion of the intestinal epithelium by *Salmonella enterica* (Baxter and Jones 2005).

In contrast, proteins up-expressed upon ZnO-NP exposure (*ZnONP-up*) are related to protein biosynthesis, especially of membrane-associated proteins: The lysin motif (LysM)-containing domain of the

uncharacterized protein Reut_A3409 suggests a membrane-associated protein of unknown function where LysM acts as a peptidoglycan hydrolase attaching secreted or membrane-associated proteins non-covalently to the membrane (Buist et al. 2008); the signal recognition particle ribonucleoprotein SRP54 functions by binding and accompanying secreted or membrane-associated proteins to the translocational machinery of the membrane (Wild et al. 2004); other *ZnONP-up* are related to purine biosynthesis (PurL), the reversible catalysis of aspartate, tyrosine and aromatic amino acids into the corresponding α-ketoacids (aspartate/tyrosine/aromatic aminotransferase), protein biosynthesis (GTP-ase translation elongation factor), and DNA integration (integrase). The identification of the membrane-associated *ZnONP-up* is significant because it suggests that cell membranes may be the primary site of damage, but also because it is consistent with the observed disruption of *Escherichia coli* cell membranes by silver nanoparticles (Ag-NPs), where an increased accumulation of precursors of membrane-associated proteins was observed (Lok et al. 2006) and by membrane disruption in *E. coli* by di(ethylene glycol)- and poly (vinylpyrolidone)-stabilized ZnO-NPs (Brayner et al. 2006; Zhang et al. 2007). However, unlike the activity of Ag-NPs towards *E. coli*, we have demonstrated a clear difference in the mode of toxicity between the nanomaterial and the free ion, the above-mentioned ZnO-NP studies do not make a comparison with free Zn(II). This study therefore supports cell membrane damage as a principle mechanism for the observed toxicity associated with a wide range of nanomaterials to bacteria (Neal 2008).

Regulation of new products requires a thorough understanding of the potential stresses that the product will place on the environment following disposal. A comprehensive evaluation of such stress is not possible without a proper characterization of the materials. With regard to nanomaterials, one of the key questions is whether they can be considered as free ions, or whether they are indeed a totally new class of potential environmental stressors. As we have demonstrated, standard chemical analyses including X-ray diffraction, FT-Raman spectroscopy and ICP-MS are unable to discern the difference between the nanomaterial suspension and zinc salts such as Zn-OAc. This is in part due to the very high concentration of acetate used to stabilize the nanomaterial, and in part due to the very small size of the ZnO-NPs. A potential conclusion from chemical analyses would be that the nanomaterial suspension is essentially similar to Zn-OAc and should be regulated as such. However, the response of bacteria to the nanomaterial compared to Zn-OAc clearly demonstrates that the two Zn forms are significantly different, principally in the bioavailability of Zn(II). This suggests that bio-reporters of metal bioavailability (Kelly et al. 2004; Peca et al. 2008; Aruoja et al. 2009; Ivask et al. 2009) may be a more reliable approach to assessing the likely mode of toxicity of new nanomaterials upon environmental release. An initial step in construction of bio-reporter strains is identification of key responding proteins (and genes). Our proteome analyses identify both SRP54 (Reut_A2947) and LysM-containing Reut_A3409 as potential indicators of cell damage by nanomaterials which do not apparently accumulate under Zn(II) toxicity. It is therefore possible to postulate that microbial bio-reporters could be used to establish not only the presence of metal ions associated with nanomaterials, but also identify the principal mode of toxicity of new nanomaterials in a rapid and reliable manner.

Acknowledgements

The authors are grateful to Keith Goulding and an anonymous reviewer for helpful criticism of the original manuscript. Any opinions, findings, conclusions or recommendations expressed in this material are those of the authors and do not necessarily reflect the views of the EPA. This work has not been subjected to EPA review and no official endorsement should be inferred.

Declaration of interest: Rothamsted Research receives grant-aided support from the Biotechnology and Biological Sciences Research Council of the UK. Major funding was provided by the U.S. Environmental Protection Agency's (EPA) Science to Achieve Results (STAR) Grant No. RD832530. Partial support was also provided by EPA STAR grant RD834574 and by the Natural Environment Research Council of the UK through grant NE/H013679/1. The authors report no conflict of interest. The authors alone are responsible for the content and writing of the paper.

References

Ambrožič G, Škapinb SD, žigona M, Orel ZC. 2010. The synthesis of zinc oxide nanoparticles from zinc acetylacetonate hydrate and 1-butanol or isobutanol. J Colloid Interface Sci 346:317–323.

Aruoja V, Dubourguier HC, Kasemets K, Kahru A. 2009. Toxicity of nanoparticles of CuO, ZnO and TiO2 to microalgae Pseudokirchneriella subcapitata. Sci Tot Environ 407:1461–1468.

Baxter AM, Jones BD. 2005. The fimYZ genes regulate Salmonella enterica serovar typhimurium invasion in addition to Type 1 fimbrial expression and bacterial motility. Infect Immun 73:1377–1385.

Beard SJ, Hughes MN, Poole RK. 1995. Inhibition of the cytochrome bd-terminated NADH oxidase system in Escherichia coli K-12 by divalent metal cations. FEMS Microbiol Lett 131:205–210.

Ben Yahia S, Znaidi L, Kanaev A, Petitet JP. 2008. Raman study of orientated ZnO thin films deposited by sol-gel method. Spectrochim Acta A: Mol Biomol Spectrosc 71:1234–1238.

Bradford MM. 1976 A rapid and sensitive method for the quantitation of microgram quantities of protein utilizing the principle of protein-dye binding. Anal Biochem 72:248–254.

Brayner R, Ferrari-Iliou R, Brivois N, Djediat S, Benedetti MF, Fiévet F. 2006. Toxicological impact studies based on Escherichia coli bacteria in ultrafine ZnO nanoparticles colloidal medium. Nano Lett 6:866–870.

Brunner TJ, Wick P, Manser P, Grass RN, Limbach LK, Bruinink A, Stark WJ. 2006. In vitro cytotoxicity of oxide nanoparticles: Comparison to asbestos, silica, and the effect of particle solubility. Environ Sci Technol 40:4374–4381.

Buist G, Steen A, Kok J, Kuipers OP. 2008. LysM, a widely distributed protein motif for binding to (peptido)glycans. Mol Microbiol 68:838–847.

Candiano G, Bruschi M, Musante L, Santucci L, Ghiggeri GM, Carnemolla B, Orecchia P, Zardi L, Righetti PG. 2004. Blue silver: A very sensitive colloidal Coomassie G-250 staining for proteome analysis. Electrophoresis 25:1327–1333.

Cheng Z-Y, Duan J, Hao Y-A, McConkey BJ, Glick BR. 2009. Identification of bacterial proteins mediating the interactions between Pseudomonas putida UW4 and Brassica napus (canola). Mol Plant-Microbe Interact 22:686–694.

Derfus AM, Chan WCW, Bhatia SN. 2004. Probing the cytotoxicity of semiconductor quantum dots. Nano Lett 4:11–18.

Don RH, Pemberton JM. 1981. Properties of six pesticide degradation plasmids isolated from Alcaligenes paradoxus and Alcaligenes eutrophus. J Bacteriol 145:681–686.

Franklin NM, Rogers NJ, Apte SC, Batley GE, Gadd GE, Casey PS. 2007. Comparative toxicity of nanoparticulate ZnO, bulk ZnO, and ZnCl2 to a freshwater microalga (Pseudokirchneriella subcapitata): The importance of particle solubility. Environ Sci Technol 41:8484–8490.

Ivask A, Rõlova T, Kahru A. 2009. A suite of recombinant luminescent bacterial strains for the quantification of bioavailable heavy metals and toxicity testing. BMC Biotech 9(41) (DOI:10.1186/1472-6710-9-41).

Kasahara M, Anraku Y. 1974. Succinate and NADH oxidase systems of Escherichia coli membrane vesicles: Mechanism of selective inhibition of the system by zinc ions. J Biochem 76:967–976.

Karlsson HL, Cronholm P, Gustafsson J, Moller L. 2008. Copper oxide nanoparticles are highly toxic: A comparison between metal oxide nanoparticles and carbon nanotubes. Chem Res Toxicol 21:1726–1732.

Kelly CJ, Tumsaroj N, Lajoie CA. 2004. Assessing wastewater metal toxicity with bacterial bioluminescence in a bench-scale wastewater treatment system. Wat Res 38:423–431.

Kim HW, Kebede M, Kim HS. 2010. Structural, Raman, and photoluminescence characteristics of ZnO nanowires coated with Al-doped ZnO shell layers. Curr Appl Phys 10:60–63.

Kimura E. 1993. Roles of zinc(II) in zinc enzymes. Pure Appl Chem 65:355–359.

Lok C-N, Ho C-M, Chen R, He Q-Y, Yu W-Y, Sun H, Tam PK-H, Chiu J-F, Che C-M. 2006. Proteomic analysis of the mode of antibacterial action of silver nanoparticles. J Proteome Res 5:916–924.

Lowry OH, Rosebrough NJ, Farr AL, Randall RJ. 1951. Protein measurement with the Folin phenol reagent. J Biol Chem 193:265–275.

Nakano S, Fukaya M. 2008. Analysis of proteins responsive to acetic acid in Acetobacter: Molecular mechanisms conferring acetic acid resistance in acetic acid bacteria. Int J Food Microbiol 125:54–59.

Neal AL. 2008. What can be inferred from bacterium-nanoparticle interactions about the potential consequences of environmental exposure to nanoparticles? Ecotoxicology 17:362–371.

Peca L, Kos PB, Mate Z, Farsang A, Vass I. 2008. Construction of bioluminescent cyanobacterial reporter strains for detection of nickel, cobalt and zinc. FEMS Microbiol Lett 289:258–264.

Pérez-Pantoja D, de la Inglesia R, Pieper DH, González B. 2008. Metabolic reconstruction of aromatic compounds degradation from the genome of the amazing pollutant-degrading bacterium Cupriavidus necator JMP134. FEMS Microbiol Rev 32:736–794.

Pötter M, Madkour MH, Mayer F, Steinbüchel A. 2002. Regulation of phasin expression and polyhydroxyalkanoate (PHA) granule formation in Ralstonia eutropha H16. Microbiology-SGM 148:2413–2426.

Steinbüchel A, Schlegel HG. 1989. Excretion of pyruvate by mutants of Alcaligenes eutrophus, which are impaired in the accumulation of poly(β-hydroxybutyric acid) (PHB), under conditions permissive for synthesis of PHB. Appl Microb Biotechnol 31:168–175.

Studer AM, Limbach LK, van Duc L, Krumeich F, Athanassiou EK, Gerber LC, Moch H, Stark WJ. 2010. Nanoparticle cytotoxicity depends upon intracellular solubility: Comparison of stabilized copper metal and degradable copper oxide nanoparticles. Toxicol Lett 197:169–174.

Respaske R, Respaske C. 1976. Quantitative requirements for exponential growth of Alcaligenes eutropha. Appl Environ Microbiol 32:585–591.

Samy El-Shall M, Graiver D, Pernisz U. 1995 Synthesis and characterization of nanoscale zinc oxide particles: I. Laser vaporization/condensation technique. Nanostruct Mater 6:297–300.

Yang RD, Tripathy S, Li Y, Sue H-J. 2005. Photoluminescence and micro-Raman scattering in ZnO nanoparticles: The influence of acetate adsorption. Chem Phys Lett 411:150–154.

Wild K, Rosendal KR, Sinning I. 2004. A structural step into the SRP cycle. Mol Microbiol 53:357–363.

York GM, Junker BH, Stubbe JA, Sinskey AJ. 2001. Accumulation of the PhaP phasin of Ralstonia eutropha is dependent on production of polyhydroxybutyrate in cells. J Bacteriol 183:4217–4226.

Zhang L, Jiang Y, Ding Y, Povey M, York D. 2007. Investigation into the antibacterial behaviour of suspensions of ZnO nanoparticles (ZnO nanofluids). J Nanopart Res 9:479–489.

Zor T, Selinger Z. 1996. Linearization of the Bradford protein assay increases its sensitivity: Theoretical and experimental studies. Anal Biochem 236:302–308.